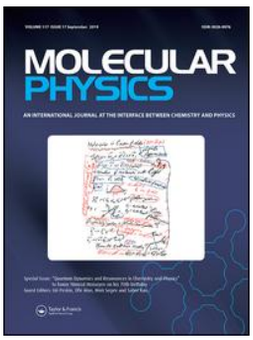

Taylor & Francis
Taylor & Francis Group

Molecular Physics

An International Journal at the Interface Between Chemistry and Physics

ISSN: (Print) (Online) Journal homepage: https://www.tandfonline.com/loi/tmph20

Charge-transfer-to-solvent states provide a sensitive spectroscopic probe of the local solvent structure around anions

Ronit Sarangi, Kaushik D. Nanda & Anna I. Krylov

To cite this article: Ronit Sarangi, Kaushik D. Nanda & Anna I. Krylov (2022): Charge-transfer-to-solvent states provide a sensitive spectroscopic probe of the local solvent structure around anions, Molecular Physics, DOI: 10.1080/00268976.2022.2148582

To link to this article: https://doi.org/10.1080/00268976.2022.2148582

MOLECULAR PHYSICS e2148582
https://doi.org/10.1080/00268976.2022.2148582

Taylor & Francis
Taylor & Francis Group

MEMORIAL ISSUE FOR NICK BESLEY

Charge-transfer-to-solvent states provide a sensitive spectroscopic probe of the local solvent structure around anions

Ronit Sarangi, Kaushik D. Nanda and Anna I. Krylov

Department of Chemistry, University of Southern California, Los Angeles, CA, USA

ABSTRACT

This computational study characterises charge-transfer-to-solvent (CTTS) states of aqueous thiocyanate anion using equation-of-motion coupled-cluster methods combined with electrostatic embedding quantum mechanics/molecular mechanics (QM/MM) scheme. Equilibrium sampling was carried out using classical molecular dynamics (MD) with standard force-fields and QM/MM *ab initio* molecular dynamics (AIMD) using density functional theory. The two calculations yield significantly different local structure around solvated SCN^-. Because of the diffuse character of CTTS states, they are very sensitive to the local structure of solvent around the solute and its dynamic fluctuations. Owing to this sensitivity, the spectra computed using MD and AIMD based snapshots differ considerably. This sensitivity suggests that the spectroscopy exploiting CTTS transitions can provide an experimental handle for assessing the quality of force-fields and density functionals. By combining CTTS-based spectroscopies with reliable theoretical modeling, detailed microscopic information of the solvent structure can be obtained. We present a robust computational protocol for modeling spectra of solvated anions and emphasise the use of an *ab initio* characterization of individual electronic transitions as CTTS or local excitations.

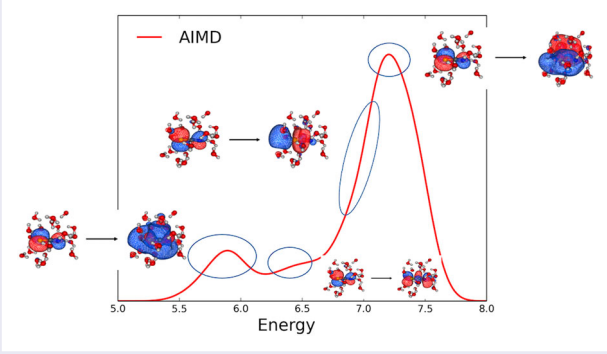

ARTICLE HISTORY
Received 31 August 2022
Accepted 13 November 2022

1. Introduction

Understanding the microscopic origins of ion-specific macroscopic properties of solutions such as surface tension, adsorption enthalpies and free energies, protein solubility, and chaotropicity has motivated intense research efforts, owing to their importance in biology [1], interfacial and atmospheric chemistry [2], electrochemistry [3], water purification and desalination [4], biofuel production [5, 6], pharmaceutical and biomedical applications [7], and more. The microscopic understanding critically depends on the characterization of the solvation environment of ions in the bulk or at interfaces. Spectroscopic techniques that are sensitive to the local solvent structure around ions, therefore, can serve as a tool for microscopic characterization of these ion-specific properties.

Small anions such as halides, hydroxide, and thiocyanate do not support bound excited electronic states in the gas phase. When solvated, they exhibit broad, featureless bands in the deep UV ($>$ 5 eV) region. These bands, which are called charge-transfer-to-solvent

CONTACT Anna I. Krylov krylov@usc.edu Department of Chemistry, University of Southern California, Los Angeles, CA 90089, USA

Supplemental data for this article can be accessed here. https://doi.org/10.1080/00268976.2022.2148582

(CTTS) excitations [8–10], arise due to the excitation of an electron into a solvent cavity, sufficiently close to the molecular core to have a non-zero oscillator strength. The CTTS states act as precursors to solvated electrons [11–16]. Because the CTTS excitations are solvent supported, they are highly sensitive to the local arrangement of the solvent around the anion and factors that can affect solvent structure, such as temperature, pressure, and presence of other solvated species [10, 17]. Hence, these states can serve as a basis for spectroscopic techniques aiming to probe local solvent structure and its dynamical fluctuations.

Many studies of CTTS states have employed UV–visible (UV–vis) spectroscopy [8–10, 18–22]. Recently, applications of two-photon absorption (2PA) and surface-sensitive nonlinear spectroscopies such as second harmonic generation, electronic sum-frequency generation (SFG), and vibrational SFG to probe anions (such as halides and thiocyanate) in the bulk and at air–liquid interfaces have been reported [23–27]. Supported by robust *ab initio* modeling, these spectroscopies can exploit CTTS transitions and help to elucidate the local solvent structure around anions. A few computational studies for modeling such spectroscopic experiments have been reported [21, 28], however, robust computational protocols based on high-level electronic structure methods are scarce.

Several studies have investigated the CTTS states in a variety of anion–solvent systems experimentally and computationally [9, 18–22, 29, 30]. In particular, the CTTS transitions of aqueous iodide [11, 20, 31–34] have garnered considerable attention. In a series of landmark papers [11–13], Sheu and Rossky simulated this system and its dynamical evolution, including the generation of solvated electrons, using a hybrid QM/MM (quantum mechanics/molecular mechanics) approach. Bradforth and Jungwirth [21] carried out a full *ab initio* calculation of energies and wave functions of the CTTS states and showed that although the long-range solvent polarization provides a dominant contribution to the binding energy of the CTTS states, it can be captured by QM/MM calculations using fixed point charges. By using MP2 to describe the solute (iodide) and point charges to describe the solvent, they were able to compute the CTTS band within $\sim$0.4 eV from the experiment. Recently, Herbert and co-workers reported calculations of the iodide CTTS bands within 0.1 eV from the experiment using a projection-based embedding scheme within the time-dependent density functional theory (DFT) [28].

Here, we focus on a more complex system, the aqueous thiocyanate anion. $SCN^-_{(aq)}$ is one of the most chaotropic ions in the Hofmeister series, i.e., it disrupts the hydrogen-bonding network of water significantly [35, 36]. Its solvation shell is highly asymmetric and has an eggshell-like shape, with a larger radius around the sulfur end [37]. It is sparsely hydrated in the bulk and shows preference for interfaces, which makes it suitable for surface-sensitive spectroscopies [23, 24, 26]. These features of $SCN^-_{(aq)}$ render it an interesting model system for studying bulk and surface CTTS states.

The room-temperature CTTS UV–vis spectra of $SCN^-_{(aq)}$ exhibit two major peaks at 5.78 eV and 6.86 eV, with a hint of a third (strong) peak around 7.14 eV [19]. However, neither the band positions nor their assignment has been backed up by computational modeling. To reliably model UV–vis spectra of solvated anions, one needs to use a high-level electronic structure method capable of treating local, diffuse, and charge-transfer (CT) transitions accurately and on an equal footing, preferably, wave-function based, although successful applications of DFT have been reported [28]. The simulations require sufficiently diffuse basis sets and accurate description of the solvent structure and its thermal fluctuations around the anion.

Modeling spectroscopy in the condensed phase requires reliable sampling over equilibrium trajectories to incorporate thermal structural fluctuations. Here, we perform such averaging by selecting structures (snapshots) from two different treatments of equilibrium dynamics. With the two sets of structures, we compute two UV–vis spectra employing a quantum/classical (QM/MM) embedding scheme based on a high-level electronic structure method. By comparing these two spectra with the experimental spectrum and by characterizing individual excitations by a variety of electronic descriptors, we developed a robust, computationally feasible protocol for simulating the UV–vis spectrum of $SCN^-_{(aq)}$ with a high-level *ab initio* method. We envision that this protocol will serve as a basis for future simulations of higher-order nonlinear spectra of $SCN^-_{(aq)}$ and other solvated anions.

The first set of snapshots was obtained using classical molecular dynamics (MD) with a standard non-polarizable force-field. In the MD simulations, we used TIP3P water [38] and the force-field parameters for sodium thiocyanate of Tesei *et al.* [39], which were reported to perform well for modeling both bulk and interfacial solvation. The second set was obtained using QM/MM *ab initio* MD (AIMD) with a high-quality density functional (ωB97X-D) [40, 41]. This choice was in part motivated by the results of Baer and Mundy [42], who studied the dynamics of bulk and interfacial anions (including thiocyanate) using the BLYP functional with Grimme's dispersion.

We computed the UV–vis spectra for the two sets of snapshots using the high-level equation-of-motion

coupled-cluster method with single and double excitations (EOM-EE-CCSD) [43, 44] within a QM/MM embedding scheme, following our previous studies [45–47]. The computational cost of EOM-EE-CCSD scales as $\mathcal{O}(N^6)$ with system size, which limits the size of the QM system. Thus, we developed a general protocol for balancing accuracy versus costs in calculations of CTTS states with such high-level QM methods.

In their study of CTTS excitations of iodide in bulk water and water clusters, Bradforth and Jungwirth [21] concluded that there is little advantage in treating the waters even in the first solvation shell quantum mechanically. Our results, in contrast, indicate that anions such as SCN^-_{aq}, which have a non-spherical solvation shell and strongly perturb the solvent structure, require much more sophisticated treatment to achieve a quantitative agreement between theory and experiment. We show that a robust description of the highly diffuse excited states in these systems requires a QM treatment of at least two solvation shells around the anion.

We then analyzed structural parameters, such as the radial distribution functions (RDFs) around the solute atoms, compared the computed RDFs with the experimentally derived ones and with each other, and illustrated the strong sensitivity of the CTTS bands to the local solvent structure around $SCN^-_{(aq)}$, which is, in turn, sensitive to the quality of interaction potentials (force fields or functionals). By juxtaposing the two sets of simulations, our results indicate that spectroscopies targeting CTTS transitions offer an experimental probe of the quality of force fields or density functionals.

To elucidate how the different local structures obtained from the two equilibrium sampling protocols impact individual excitations, we characterised these electronic transitions by computing and visualizing natural transition orbitals (NTOs) [48–50]. For solvated anionic systems, however, visualizing the NTOs is not sufficient to clearly distinguish between intramolecular excitations and CTTS transitions due to the mixing of local and CT excitations at some configurations. Moreover, visual inspection of NTOs for each snapshot is not practical. Therefore, we augmented the NTO analysis for the selected snapshots with quantitative descriptors such as hole, particle, and exciton sizes, computed using the corresponding reduced one-particle transition density matrices (1PTDMs). Together, NTO visualization and statistical analysis of the descriptors provide a comprehensive toolkit for characterizing CTTS and intramolecular transitions in solvated anionic systems.

The structure of this paper is as follows. The next section describes computational protocols with additional details given in the Supplemental Information (SI). In Section 3, we discuss the results and examine the structural differences between the MD and AIMD calculations, illustrating how these differences are reflected in the UV–vis spectra.

2. Computational details

2.1. Molecular dynamics

MD simulations were performed with NAMD [51], version 2.14, using the initial configuration generated by Packmol [52]. The system comprises an SCN^- ion solvated in 1,347 water molecules and one Na^+ counterion in a periodic cubic box with a side of 34.4 Å. The water molecules were described by TIP3P model and the parameters for Na^+ and SCN^- were taken from Ref. [39]. A timestep of 1 fs was chosen for the simulation. The waters were made rigid using the SETTLE algorithm. The electrostatic interactions were computed using the Particle–Mesh Ewald method with a 14 Å cutoff for long-range interactions. Following initial energy minimization, the system was equilibrated for 500 ps in an NVT ensemble maintained at 300 K using the Langevin thermostat. This was followed by 3 ns of production runs in NPT ensemble with 1 atm pressure maintained using the Nosé–Hoover method. From this MD trajectory, we collected 80 snapshots separated by 2.5 ps for the calculations of the spectra.

2.2. Ab initio molecular dynamics

Seven snapshots from the MD run were chosen as the initial configurations for the AIMD simulations. In these simulations, the system was divided into the QM and MM parts. The QM part, which included SCN^- and 20 nearest waters, was described by ωB97X-D/6-31+G*. The waters for the QM part were selected based on the distance from the carbon atom of SCN^-. The MM part was described by TIP3P waters. The van der Waals parameters for the SCN^- and Na^+ ions were taken from Ref. [39]. The QM–MM interaction was described by electrostatic embedding. The system was equilibrated for 1 ps in an NVE ensemble, followed by 2.5 ps production run in an NVT ensemble with the 1 fs timestep. The temperature was maintained at 300 K using the Langevin thermostat and the long-range interactions were calculated using Ewald's summation. A total of 84 snapshots were taken at 200 fs intervals from the trajectories for excitation-energy calculations. We note that unless an adaptive QM/MM scheme is used, the quantum waters can diffuse away from SCN^- in the course of the simulation. On analysing our snapshots we found that such exchange between quantum and classical waters around

SCN^- was minimal, affecting just a few waters from the outer solvation shell (see Figure S5 in the SI).

2.3. Calculation of excited states

We computed excited states and energies using a hybrid QM/MM approach with electrostatic embedding with the EOM-EE-CCSD method [43, 44] for the QM treatment. The MM water molecules were described as TIP3P point charges with a Gaussian blur. In order to establish optimal protocol for these calculations, we investigated the convergence of the spectra with respect to the number of waters in the QM region, basis set, and the number of excited states computed; in these exploratory calculations, we used the configuration interaction singles (CIS) method. We briefly describe the resulting protocol below; more details are given in the SI.

We determined that the CIS spectrum needs at least 20 waters in the QM region for excitation energies to converge within 0.01 eV, as shown in Figure S1 in the SI. The first solvation shell of SCN^- contains 8 waters; 20 waters correspond roughly to two solvation shells. Given the importance of Pauli repulsion for these states (i.e. without it, the electron density can extend too far into the solvent), it is not surprising that at least two solvation shells are needed for an adequate description of the CTTS bands. For each snapshot, the QM system was determined by choosing 20 water molecules that are closest to the carbon atom of the anion. Because of the potential exchange between quantum and classical waters in the course of AIMD simulation, it means that the QM system in the calculation of spectra slightly differs from the QM system in the AIMD snapshot; our analysis indicates that these adjustments only affected a small number of snapshots and only affected the outermost water molecules.

The basis-set convergence analysis (see Figure S2 in the SI) indicates that a mixed basis set 6-31+G*/6-31G (wherein SCN^- and eleven nearest waters are described by the 6-31+G* basis and the remaining nine waters are described by 6-31G) yields excitation energies that are blue-shifted by only 0.1 eV relative to our reference calculations in which SCN^- and 24 nearest waters are described by the aug-cc-pVDZ basis. The mixed basis set contains almost three times fewer basis functions than the full aug-cc-pVDZ (431 versus 1,111), which affords significant savings in the EOM-EE-CCSD calculations. To test the effect of additional diffuse basis functions, we also carried out calculations with the above basis augmented with additional *s* and *p* diffuse functions on SCN^- and observed only minor (< 0.1 eV) changes in excitation energies, which indicates that the diffuse basis functions on the QM waters are sufficient to describe the CTTS states.

In the production-level EOM-EE-CCSD/MM calculations, we computed the lowest eight excitations (see Figure S3). The CCSD and EOM-CCSD steps were executed in single precision, which affords a significant cut in the memory and computational time requirements compared to the double-precision execution, while introducing negligible errors [53]. The core orbitals were frozen in these calculations. We also froze all virtual orbitals with energies above 2.5 hartree; this resulted in significant reduction of the computational cost while introducing negligible errors of the order of < 0.01 eV in excitation energies.

In summary, the final protocol used for the production-level EOM-EE-CCSD/MM calculations is as follows:

(1) QM Region: SCN^- + 20 nearest waters;
(2) Mixed basis set: 6-31+G* on SCN^- and 11 nearest waters, 6-31G on the rest;
(3) MM waters: TIP3P point charges with a Gaussian blur;
(4) Excited states requested: 8;
(5) All core orbitals and virtual orbitals above 2.5 hartree in energy were frozen;
(6) CCSD and EOM-EE-CCSD calculations were executed in single precision;
(7) The stick spectra from the MD and AIMD snapshots were convoluted using normalised Gaussian functions with a full width at half maxima (FWHM) of 0.1177 eV and added together to produce the cumulative spectrum.

Sample inputs for the QM/MM AIMD and EOM-EE-CCSD/MM jobs are provided in the SI. All AIMD and EOM-EE-CCSD/MM calculations were carried out using the Q-Chem software [54, 55].

3. Results and discussion

3.1. Equilibrium dynamics

Figure 1 shows RDFs for distances between S, C, and N atoms of the anion and the O and H atoms of the solvating waters, obtained from the MD and AIMD simulations. The RDFs for the MD simulations were computed using the last 2 ns of the production run. For the AIMD simulations, we use the average RDFs of the individual runs. Both simulations show the eggshell-like solvation shell around SCN^-, i.e. featuring different radii of the first solvation shell around each atom, with N having a tighter shell compared to S, and C having the largest radii, as

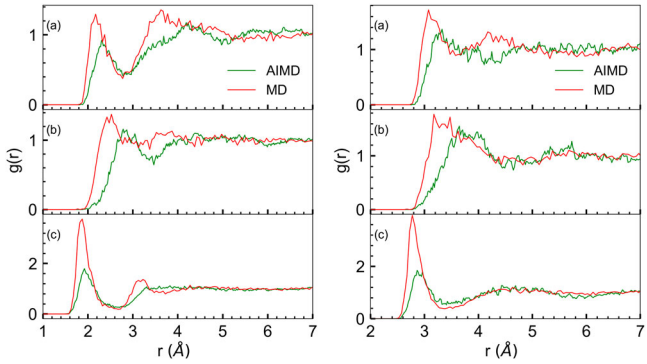

Figure 1. RDFs of H (left panel) and O (right panel) atoms on waters with respect to the (a) S, (b) C, and (c) N atoms on SCN^-, extracted from the MD and QM/MM AIMD simulations.

Table 1. Key RDF parameters extracted from MD and AIMD simulations and the experimentally derived values.

	MD		AIMD		Expt.[a]	
RDF	r_{max}, Å	n_{tot}	r_{max}, Å	n_{tot}	r_{max}, Å	n_{tot}
S–O	3.07	3.94	3.34	5.31	3.1	5.17
C–O	3.35	9.60	3.72	8.13	3.3	8.05
N–O	2.77	4.49	2.90	3.09	2.8	3.1

[a] From Ref. [56].

clearly seen in Figure 1 (right panel). This is consistent with the previous experimental and theoretical studies [42, 56].

Table 1 compares the positions of the first RDF maximum (r_{max}) and the approximate water-coordination number (n_{tot})–defined as the area under the first peak — for the computed RDFs of O atoms shown in Figure 1 to those from experimentally derived RDFs. We note that the latter should not be taken as the exact reference, because their quality depends on the underlying refinement protocols. In this case, the experimental RDFs are obtained by fitting the experimental neutron diffraction spectra using the empirical potential structure refinement technique [56]. As illustrated in the context of other structure-determination studies, using higher-level methods (such as QM/MM instead of classical MD) can noticeably affect the values of the extracted structural parameters [57–60].

The MD simulations reproduce experimental r_{max} but overestimate the total number of waters in the first solvation shell by about 2 waters. The QM/MM AIMD simulations yield better n_{tot} but overestimate the r_{max} by approximately 0.3 Å relative to the experimental values. The results in Figure 1 and Table 1 show that the MD simulations over-structure the solvent around SCN^- near the N end, as revealed by the high value at the first RDF peak. In contrast, the AIMD simulations yield fewer waters (compared to MD) in the first solvation shell and a larger radius of the shell and, therefore, yield a less structured solvent shell.

Figure 2 shows the average distances and standard deviations for the 11 nearest water molecules from the S and N ends. The waters in the AIMD snapshots are, on average, farther than in the MD snapshots; the discrepancy reduces beyond 11 waters, i.e. in the second solvation shell. It also shows the difference between the S and N ends — in the MD simulations, the closest waters to the N end show low standard deviation, meaning that they are tightly bound to the N atom in the course of the 2 ns simulation time (this is what we call over-structuring), but in the AIMD simulations the standard deviation is larger, indicating larger structural fluctuations.

One difference between the MD and QM/MM AIMD simulations is that the MM waters are frozen while the AIMD waters are allowed to vibrate in the course of dynamics. In order to assess the impact of this structural constraint on individual water molecules in the MD simulations on the local structure around the anion, we performed an additional AIMD simulation with frozen bonds and angles of water molecules using the RATTLE algorithm. Figure S6 in the SI compares the N–H and N–O RDFs of constrained water simulations with the ones from Figure 1. We observe no appreciable difference in the RDFs, which means that constraining the water bond lengths and angles is not responsible for the

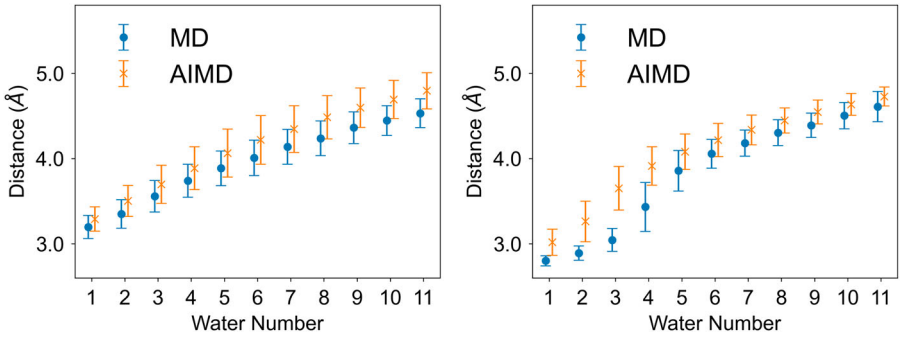

Figure 2. Average distances and standard deviations for the 11 nearest water molecules from the S (left) and N (right) ends of SCN^- extracted from the MD and AIMD simulations.

observed differences in the solvent structure around the anion.

In summary, classical MD and QM/MM AIMD yield rather different local solvent structure around SCN^-. The spectroscopic manifestation of these differences is discussed below.

3.2. UV–vis spectrum

We begin by analyzing the types and character of the excitations observed in our calculations. Figure 3 shows representative natural transition orbitals (NTOs) for low-lying EOM-EE-CCSD transitions [48–50, 61]. The hole NTO is always of HOMO or HOMO-1 (of SCN^-) character and the character of transitions can be assigned based on the shape of the particle NTOs. As we show below, the lowest states are dominated by intramolecular Δ-like character (arising from $\pi \rightarrow \pi^*$ transition), and the higher bands are dominated by the three CTTS state of *s*- and *p*-like characters. We note that in isolated linear molecules, the $\Sigma \rightarrow \Delta$ transitions are forbidden by symmetry, however, in the asymmetric solvent environment, they become weakly allowed. As we show below, for some solvent configurations, the intramolecular and the lowest CTTS excitations can mix, giving rise to states of mixed character and intensity redistribution.

Tables S3 and S4 in the SI show NTOs and exciton descriptors [49, 61, 62] — such as the norm of 1PTDM and the participation ratio — for two representative snapshots, one from the MD and one from the AIMD simulations. Table 2 gives the average values and standard deviations for the excitation energies and oscillator strengths of the lowest eight transitions across all the snapshots sampled from the MD and AIMD simulations. These data suggest that the energy ordering and characters of states is different for MD and AIMD snapshots, as explained below.

For the MD snapshots, the oscillator strengths for excitations 1, 2, and 3 show very small values that are approximately an order of magnitude lower than those for the higher transitions. The NTO analysis of these

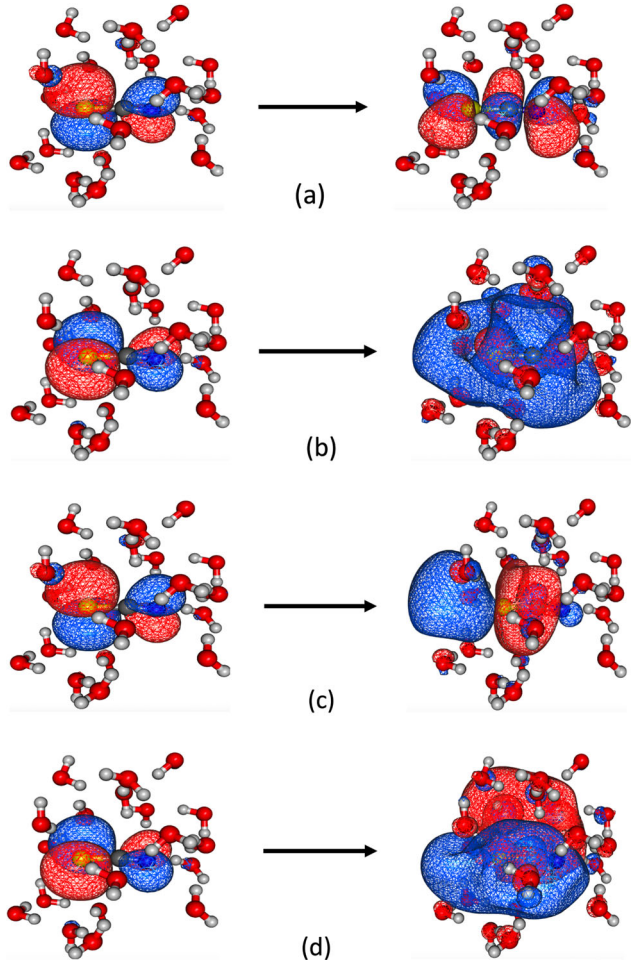

Figure 3. NTOs for the lowest excited states from EOM-EE calculations: (a) intramolecular Δ state; (b) *s*-type CTTS state; (c) *p*-type CTTS state; (d) *p*-type CTTS state.

Table 2. Raw data for excitation energies (E_{ex}, eV) and oscillator strengths (f).

	MD		AIMD	
#	E_{ex}	f	E_{ex}	f
1	5.91 ± 0.17	0.001 ± 0.002	5.79 ± 0.20	0.024 ± 0.015
2	6.05 ± 0.15	0.004 ± 0.004	5.93 ± 0.19	0.030 ± 0.012
3	6.17 ± 0.15	0.003 ± 0.004	6.34 ± 0.14	0.010 ± 0.012
4	6.49 ± 0.16	0.026 ± 0.017	6.47 ± 0.15	0.013 ± 0.009
5	6.62 ± 0.17	0.024 ± 0.012	6.58 ± 0.16	0.011 ± 0.010
6	7.22 ± 0.16	0.212 ± 0.186	6.91 ± 0.17	0.078 ± 0.117
7	7.35 ± 0.16	0.157 ± 0.152	7.05 ± 0.19	0.036 ± 0.060
8	7.51 ± 0.13	0.356 ± 0.227	7.32 ± 0.17	0.252 ± 0.162

three transitions reveals the intramolecular character of these Δ-like transitions with the particle NTOs resembling those shown in Table S3 and localised on SCN^-. For these snapshots, transitions 4 and 5 are CTTS transitions with an *s*-like particle NTOs. Transitions 6 and 7 have a p_z-like particle NTO aligned along the molecular axis. In contrast, transition 8 has a p_x-like particle NTO that resembles a *p* orbital perpendicular to the molecular axis. The smaller standard deviations in oscillator strengths for the lowest transitions are also consistent with their intramolecular character, compared to those for higher-lying CTTS transitions, which are more sensitive to the fluctuations of the local solvent structure in the course of equilibrium dynamics.

In contrast, for the AIMD snapshots, the averages and standard deviations for oscillator strengths are lowest for excitations 3, 4, and 5 and are about ∼50% lower than those for transitions 1 and 2 (see Table 2). Thus, it is not possible to distinguish the intramolecular Δ-like transitions from the CTTS transitions based on the oscillator strengths alone. Table S4 presents the NTO analysis for a representative AIMD snapshot. Visually, the NTO analysis suggests that transitions 1 and 2 are CTTS transitions with *s*-like particle NTOs. Thus, the energy ordering of excited states is different for snapshots from MD and AIMD simulations. Further, NTOs for transitions 3, 4, 5, 6, and 7 reveal mixed intramolecular and p_z-like CTTS character, which explains the non-negligible oscillator strengths for these transitions, in contrast to the pure intramolecular transitions from the MD snapshot. NTOs of transition 8 characterise it as a p_x-like CTTS transitions with a *p*-like particle NTO perpendicular to the molecular axis. Thus, simple visualization of NTOs for AIMD snapshots is not sufficient to clearly differentiate between the states dominated by CTTS or local transitions.

In order to quantify inter- and intra-molecular character of the transitions across all snapshots, we computed the averaged values and standard deviations for *ab initio* descriptors [48, 61, 62] such as the hole, particle (electron), and exciton sizes (d_h, d_e, and d_{exc}, respectively). The results are summarized in Figure 4. d_{exc} — defined as the root-mean-square (RMS) electron–hole distance — quantifies the extent of delocalization and charge resonance. For inter-fragment transitions such as the CTTS transitions, average d_{exc} and d_e are expected to be larger than those for localized intramolecular transitions. This is confirmed in Figure 4; transitions 1, 2, and 3 for the MD snapshots and transitions 3, 4, and 5 for the AIMD snapshots show much smaller average exciton and particle sizes compared to those for the other transitions. The average hole sizes do not vary much, in contrast to

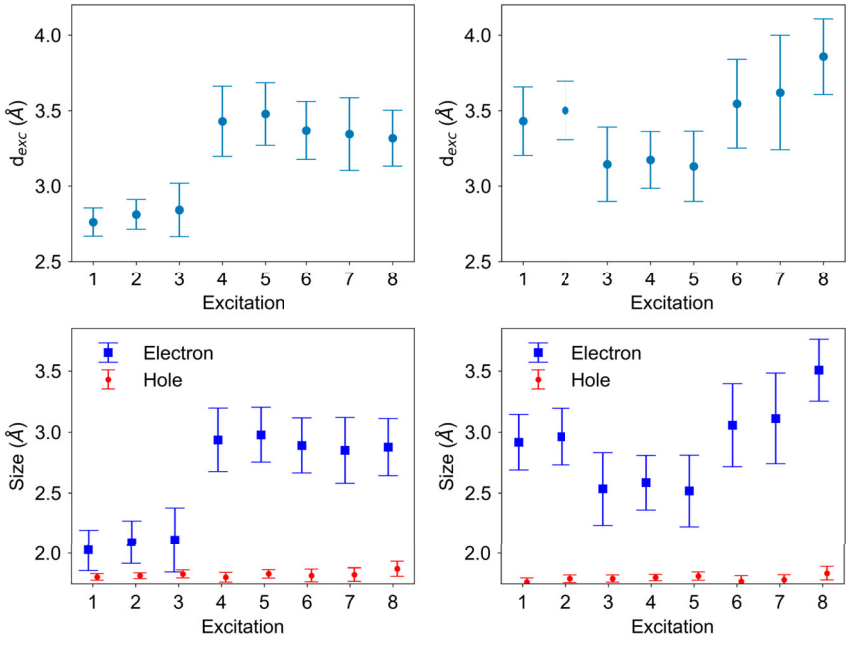

Figure 4. Average exciton, hole, and particle sizes and their standard deviations for MD (left) and AIMD (right) snapshots.

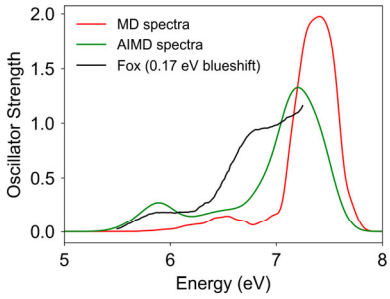

Figure 5. Comparison of aqueous SCN^- spectra calculated at $T = 300$ K using MD and AIMD with the experimental spectrum (at $T = 274$ K) from Ref. [19].

the particle and exciton sizes, across these transitions, as also expected from the visualization of NTOs. Further, compared to MD, AIMD leads to larger exciton and particle sizes, which can be attributed to larger transient cavities around SCN^- in the AIMD simulations. These differences in wave-function descriptors are, therefore, consistent with the differences in computed RDFs in Figure 1. We note that large dynamic fluctuations of the electronic descriptors of the CTTS states reflect their sensitivity to the shape of the transient cavities around the anion. Thus, these descriptors provide theoretical means to quantify this previously noted feature of the CTTS states [21, 33].

Figure 5 shows the spectra computed using snapshots from MD and AIMD simulations and compares them with the experimental absorption spectrum of aqueous tetramethylammonium thiocyanate by Fox *et al.* [19]. We note that the experimental spectrum was recorded at 274 K, whereas the simulations were carried out at 300 K. Based on the data from Ref. [19], at room temperature, the position of the lowest band should blue shift by 0.01 eV and the position of the second band red shifts by 0.06 eV.

Fox *et al.* reported four sets of numbers (see Table S2). One set corresponds to the low-temperature spectrum ($T = 274$ K, the one shown in Figure 5), but the three other sets presumably correspond to 298 K and the reason for the discrepancies between them is not clear. Therefore, the comparison between the theory and experiment is not straightforward. In addition to this issue, we note that the experimental spectrum stops while the band intensity is still rising, so the estimated position and the intensity of the third peak may not be reliable. Moreover, the experimental paper also cautions that due to the low intensity of the lowest band, the fitting was ambiguous.

Fox *et al.* assigned the peaks at 5.78 eV and 6.86 eV as CTTS excitations and provided evidence of a third peak at 7.14 eV. The assignment of the bands was based on temperature and solvent sensitivity of the peaks [19]. Table 3 summarises the computed peak positions with the corresponding experimental values (we use the set of numbers given in the Conclusion section of Ref. [19]). The theoretical values in Table 3 were obtained by fitting the computed spectra with four gaussians (see SI).

Table 3. Comparison of peak positions (eV) of computed and experimental UV–vis spectra of $SCN^-_{(aq)}$.

Peak	Character	MD	AIMD	Expt.[a]
1	*s*-type CTTS	6.52	5.89	5.78
2	*p*-type CTTS	7.24	6.93	6.86
3	*p*-type CTTS	7.47	7.24	7.14
4	Intramolecular	5.90	6.45	–

[a] From Ref. [19].

Relative to the MD spectrum, the *s*-type CTTS excitation is red-shifted by ~0.6 eV, *p*-type CTTS is red-shifted by ~0.3 eV, and the intramolecular excitation is blue-shifted by ~0.5 eV in the AIMD spectrum. This indicates that the CTTS-type excitations are stabilised in the QM/MM AIMD simulations, thereby, shifting to lower energies. Table 3 also shows that the AIMD peaks match well with the experimental peaks; the discrepancies in the peak positions are within the error bars of the quantum-chemistry method.

Finally, we correlate the structural differences in solvation around SCN^- in the MD and AIMD simulations with the differences in the UV–vis spectra. The AIMD simulations show a higher r_{max} than MD simulations, which means that the first solvation shell is larger in the former. This stabilises the diffuse CTTS states by reducing the Pauli repulsion between the extended electron density of the CTTS state and the surrounding water molecules. We also argue that the diffuse *s*-type CTTS excitations are affected more by this stabilization than the directional *p*-type CTTS excitations, as indicated by a larger red shift of the *s*-type CTTS state. The blue shift for the intramolecular excitation can be explained in terms of the stabilization of these compact states by tighter solvation in the MD simulations.

4. Conclusions

We investigated the CTTS states of aqueous thiocyanate by means of high-level electronic structure calculations. We considered two equilibrium dynamics simulations for $SCN^-_{(aq)}$: force-field-based MD and hybrid QM/MM AIMD calculations. The two simulations result in rather different local structures of water around the anion. The structural parameters show that MD over-structures waters around nitrogen and overestimates the numbers of water in the first solvation shell. In contrast, AIMD

reproduces the number of waters in the first solvation shell while overestimating its radius compared to experimentally derived results. Importantly, AIMD results in a less rigid solvent shell, giving rise to larger structural fluctuations.

From the two sets of snapshots sampled from the MD and AIMD trajectories, we computed excited states using a QM/MM electrostatic embedding scheme wherein we used the EOM-EE-CCSD method for the QM treatment. We identified a convergent setup for the QM and MM subsystems in which the anion and its two solvation shells comprising 20 nearest waters are treated quantum mechanically. Our results indicate that the lowest excited states computed from the MD and AIMD snapshots show significant differences in the average peak positions and oscillator strengths, which we attributed to the different solvent structures around the anion. We augmented these results with the analysis of NTOs for these transitions. For the MD snapshots, the intramolecular and CTTS transitions are easy to distinguish by visualization of the NTOs. In contrast, we find that many transitions from the AIMD snapshots have mixed intramolecular and CTTS character. Thus, simple visualization of NTOs is insufficient for the characterization of individual transitions. Moreover, visual inspection of each snapshot from the simulations is impractical. We demonstrated that wave-function descriptors such as the hole, particle, and exciton sizes allow for a more thorough differentiation between CTTS and local transitions across all snapshots.

The computed MD and AIMD spectra are also different. We correlated the computed structural differences in the two sampling methods with the differences in the peak positions of CTTS and local transitions. The over-structuring of solvent molecules and smaller cavity around the anion computed in the MD simulations overstabilizes the intramolecular transitions on the anion but destabilises the diffuse CTTS states due to the electronic repulsion with solvated waters. We show that the computed UV–vis spectrum with the AIMD snapshots agrees reasonably well with the experimental spectrum.

Our results suggest that the force-field parameters used in our MD simulations are inadequate to describe the hydration of SCN^- anion and also present an argument in favor of the more computationally expensive AIMD methods in further studies.

In agreement to previous studies [21, 33], our results show that CTTS excitations are strongly sensitive to the local structure of water around the anion; therefore, robust modeling of spectroscopic processes involving these excitations requires an accurate description of solvation dynamics of these anions. Conversely, spectroscopies utilizing these states provide a sensitive experimental probe of both the local structure of the solvent around anionic solutes and of the quality of force fields and density functionals; we propose to explore this idea in future studies. Our observations also suggest that spectroscopies based on the CTTS transitions can be used to gain detailed insight into local structure of the solvent–if supplemented by reliable modeling. While this idea — learn about microscopic structure from simulations and use spectroscopic observables to validate the simulations — is the same as traditionally used in many spectroscopic studies, the distinction here is that for other types of electronic transitions, inhomogeneous broadening is often hiding the imperfections of the simulations. For example, in our previous studies of solvated species (CN, phenol, phenolate, thymine, glycine, water) [45–47, 63, 64], we were getting a reasonably good agreement with the experimental photoelectron spectra (and redox potentials) with equilibrium sampling using classical force fields. In contrast, strong sensitivity of the CTTS states to the shape of the transient cavities exposes the deficiencies of such theoretical models.

Our study also highlights the outstanding difficulties in condensed-phase studies. In addition to the limitations of the theoretical methods, the comparison with experimentally derived values is often not straightforward. In the context of solvated anions, we note that the quality of the experimental RDFs depends on the simulation protocols used in the structure refining procedures. The interpretation of the experimental spectra in terms of the positions and intensities of the specific bands depends on fitting procedures, and so on. In addition, the comparisons are often hindered by uncertainties in the calibration procedures, which translate into the uncertainties in the experimental intensities, and by a limited range of energies. Thus, more work is needed from both the experimental and theoretical sides in order to fully understand even such simple system as solvated SCN^-. We hope that the progress in theoretical capabilities, as illustrated by the present simulations, will inspire further experimental efforts.

In summary, we have developed a robust computational protocol for modeling the UV–vis spectrum of the aqueous thiocyanate anion and presented a toolkit for a first-principles characterization of CTTS transitions. Our strategy of developing a reliable computational protocol for modeling the UV–vis spectrum of $SCN^-_{(aq)}$ can be extended to other aqueous anionic systems and to modeling other spectroscopic signals, such as nonlinear 2PA and SFG spectra. Thus, this work lays the foundation for modeling condensed-phase spectra of anions, which involve both intra-molecular and CTTS bands, by high-level electronic structure method such as EOM-EE-CCSD.

Disclosure statement

The authors declare the following competing financial interest(s): A.I.K. is the president and a part-owner of Q-Chem, Inc.

Funding

This work was supported by the U.S. National Science Foundation (No. CHE-2154482 to A.I.K.). We also acknowledge using USC HPCC resources.

ORCID

Ronit Sarangi http://orcid.org/0000-0002-5838-003X
Kaushik D. Nanda http://orcid.org/0000-0002-3447-6678
Anna I. Krylov http://orcid.org/0000-0001-6788-5016

References

[1] Y. Zhang and P.S. Cremer, Curr. Opin. Chem. Biol. **10**, 658 (2006). doi:10.1016/j.cbpa.2006.09.020
[2] D.J. Tobias, A.C. Stern, M.D. Baer, Y. Levin and C.J. Mundy, Annu. Rev. Phys. Chem. **64**, 339 (2013). doi:10.1146/physchem.2013.64.issue-1
[3] S. Yoshimoto and K. Itaya, Annu. Rev. Anal. Chem. **6**, 213 (2013). doi:10.1146/anchem.2013.6.issue-1
[4] M.A. Shannon, P.W. Bohn, M. Elimelech, J.G. Georgiadis, B.J. Mariñas and A.M. Mayes, Nature **452**, 301 (2008). doi:10.1038/nature06599
[5] J.A. Cray, A. Stevenson, P. Ball, S.B. Bankar, E.C.A. Eleutherio, T.C. Ezeji, R.S. Singhal, J.M. Thevelein, D.J. Timson and J.E. Hallsworth, Curr. Opin. Biotechnol. **33**, 228 (2015). doi:10.1016/j.copbio.2015.02.010
[6] D.J. Timson, World J. Microbiol. Biotechnol. **36**, 89 (2020). doi:10.1007/s11274-020-02865-8
[7] L. Zongo, H. Lange and C. Crestini, ACS Omega **4**, 6979 (2019). doi:10.1021/acsomega.8b03510
[8] M. Smith and M.C.R. Symons, Trans. Faraday Soc. **54**, 338 (1958). doi:10.1039/TF9585400338
[9] G. Stein and A. Treinin, Trans. Faraday Soc. **55**, 1086 (1959). doi:10.1039/TF9595501086
[10] M.J. Blandamer and M.F. Fox, Chem. Rev. **70**, 59 (1970). doi:10.1021/cr60263a002
[11] W.S. Sheu and P.J. Rossky, Chem. Phys. Lett. **202**, 186 (1993). doi:10.1016/0009-2614(93)85263-N
[12] W.S. Sheu and P.J. Rossky, Chem. Phys. Lett. **213**, 233 (1993). doi:10.1016/0009-2614(93)85125-8
[13] W.S. Sheu and P.J. Rossky, J. Phys. Chem. **100**, 1295 (1996). doi:10.1021/jp9513531
[14] A. Staib and D. Borgis, J. Chem. Phys. **104**, 9027 (1996). doi:10.1063/1.471635
[15] R. Lian, D.A. Oulianov, R.A. Crowell, I.A. Shkrob, X. Chen and S.E. Bradforth, J. Phys. Chem. A **110**, 9071 (2006). doi:10.1021/jp0610113
[16] H. Iglev, M.K. Fischer and A. Laubereau, Pure & Appl. Chem. **82**, 1919 (2010). doi:10.1351/PAC-CON-09-12-04
[17] T.R. Griffiths and M.C.R. Symons, Trans. Faraday Soc. **56**, 1125 (1960). doi:10.1039/TF9605601125
[18] M. Luria and A. Treinin, J. Phys. Chem. **72**, 305 (1968). doi:10.1021/j100847a059
[19] M.F. Fox, C.B. Smith and E. Hayon, J. Chem. Soc. Faraday Trans **77**, 1497 (1981). doi:10.1039/f19817701497
[20] M.F. Fox and E. Hayon, J. Chem. Soc. Faraday Trans. **73**, 1003 (1977). doi:10.1039/f19777301003
[21] S.E. Bradforth and P. Jungwirth, J. Phys. Chem. A **106**, 1286 (2002). doi:10.1021/jp013068p
[22] T.W. Marin, I. Janikand and D.M. Bartels, Phys. Chem. Chem. Phys. **21**, 24419 (2019). doi:10.1039/C9CP03805A
[23] P.B. Petersen, R.J. Saykally, M. Mucha and P. Jungwirth, J. Phys. Chem. B **109**, 10915 (2005). doi:10.1021/jp050864c
[24] R.M. Onorato, D. Otten and R.J. Saykally, Proc. Nat. Acad. Sci. **106**, 15176 (2009). doi:10.1073/pnas.0904800106
[25] A.M. Rizzuto, S. Irgen-Gioro, A. Eftekhari-Bafrooei and R.J. Saykally, J. Phys. Chem. Lett. **7**, 3882 (2016). doi:10.1021/acs.jpclett.6b01931
[26] H. Mizuno, A.M. Rizzuto and R.J. Saykally, J. Phys. Chem. Lett. **9**, 4753 (2018). doi:10.1021/acs.jpclett.8b01966
[27] D. Bhattacharyya, H. Mizuno, A.M. Rizzuto, Y. Zhang, R.J. Saykally and S.E. Bradforth, J. Phys. Chem. Lett. **11**, 1656 (2020). doi:10.1021/acs.jpclett.9b03857
[28] K. Carter-Fenk, C.J. Mundy and J.M. Herbert, J. Chem. Theory Comput. **17**, 4195 (2021). doi:10.1021/acs.jctc.1c00412
[29] L. Dogliotti and E. Hayon, J. Phys. Chem. **72**, 1800 (1968). doi:10.1021/j100851a073
[30] M.R. Waterland and A.M. Kelley, J. Phys. Chem. A **105**, 8385 (2001). doi:10.1021/jp010925g
[31] J.A. Kloepfer, V.H. Vilchiz, V.A. Lenchenkov and S.E. Bradforth, Chem. Phys. Lett. **298**, 120 (1998). doi:10.1016/S0009-2614(98)01210-X
[32] A.E. Bragg and B.J. Schwartz, J. Phys. Chem. B **112**, 483 (2008). doi:10.1021/jp076934s
[33] V.T. Pham, I. Tavernelli, C.J. Milne, R.M. van der Veen, P. D'Angelo, Ch. Bressler and M. Chergui, Chem. Phys. **371**, 24 (2010). doi:10.1016/j.chemphys.2010.03.023
[34] H. Okuyama, Y. Suzuki, S. Karashima and T. Suzuki, J. Chem. Phys. **145**, 074502 (2016). doi:10.1063/1.4960385
[35] P.L. Nostro and B.W. Ninham, Chem. Rev. **112**, 2286 (2012). doi:10.1021/cr200271j
[36] L.C. Smeeton, J.C. Hey and R.L. Johnston, Inorganics **5**, 20 (2017). doi:10.3390/inorganics5020020
[37] P.E. Mason, G.W. Neilson, C.E. Dempsey, A.C. Barnes and J.M. Cruickshank, Proc. Nat. Acad. Sci. **100**, 4557 (2003). doi:10.1073/pnas.0735920100
[38] P. Mark and L. Nilsson, J. Phys. Chem. A **105**, 9954 (2001). doi:10.1021/jp003020w
[39] G. Tesei, V. Aspelin and M. Lund, J. Phys. Chem. B **122**, 5094 (2018). doi:10.1021/acs.jpcb.8b02303
[40] J.-D. Chai and M. Head-Gordon, J. Chem. Phys. **128**, 084106 (2008). doi:10.1063/1.2834918
[41] J.-D. Chai and M. Head-Gordon, Phys. Chem. Chem. Phys. **10**, 6615 (2008). doi:10.1039/b810189b
[42] M.D. Baer and C.J. Mundy, Faraday Discuss **160**, 89 (2013). doi:10.1039/C2FD20113E
[43] J.F. Stanton and R.J. Bartlett, J. Chem. Phys. **98**, 7029 (1993). doi:10.1063/1.464746
[44] A.I. Krylov, Annu. Rev. Phys. Chem. **59**, 433 (2008). doi:10.1146/physchem.2008.59.issue-1
[45] P.A. Pieniazek, S.E. Bradforth and A.I. Krylov, J. Phys. Chem. A **110**, 4854 (2006). doi:10.1021/jp0545952

[46] D. Ghosh, A. Roy, R. Seidel, B. Winter, S.E. Bradforth and A.I. Krylov, J. Phys. Chem. B **116**, 7269 (2012). doi:10.1021/jp301925k
[47] A. Sadybekov and A.I. Krylov, J. Chem. Phys. **147**, 014107 (2017). doi:10.1063/1.4990564
[48] A.V. Luzanov and O.A. Zhikol, in *Practical Aspects of Computational Chemistry I: An Overview of the Last Two Decades and Current Trends*, edited by J. Leszczynski and M.K. Shukla (Springer, Dordrecht, 2012), pp. 415–449.
[49] S.A. Bäppler, F. Plasser, M. Wormit and A. Dreuw, Phys. Rev. A **90**, 052521 (2014). doi:10.1103/PhysRevA.90.052521
[50] A.I. Krylov, J. Chem. Phys. **153**, 080901 (2020). doi:10.1063/5.0018597
[51] J.C. Phillips, R. Braun, W. Wang, J. Gumbart, E. Tajkhorshid, E. Villa, C. Chipot, R.D. Skeel, L. Kale and K. Schulten, J. Comput. Chem. **26**, 1781 (2005). doi:10.1002/(ISSN)1096-987X
[52] L. Martńez, R. Andrade, E.G. Birgin and J.M. Martínez, J. Comput. Chem. **30**, 2157 (2009). doi:10.1002/jcc.v30:13
[53] P. Pokhilko, E. Epifanovskii and A.I. Krylov, J. Chem. Theory Comput. **14**, 4088 (2018). doi:10.1021/acs.jctc.8b00321
[54] A.I. Krylov and P.M.W. Gill, WIREs: Comput. Mol. Sci. **3**, 317 (2013). doi:10.1002/wcms.1122.
[55] E. Epifanovsky, A.T.B. Gilbert, X. Feng, J. Lee, Y. Mao, N. Mardirossian, P. Pokhilko, A.F. White, M.P. Coons, A.L. Dempwolff, Z. Gan, D. Hait, P.R. Horn, L.D. Jacobson, I. Kaliman, J. Kussmann, A.W. Lange, K.U. Lao, D.S. Levine, J. Liu, S.C. McKenzie, A.F. Morrison, K.D. Nanda, F. Plasser, D.R. Rehn, M.L. Vidal, Z.-Q. You, Y. Zhu, B. Alam, B.J. Albrecht, A. Aldossary, E. Alguire, J.H. Andersen, V. Athavale, D. Barton, K. Begam, A. Behn, N. Bellonzi, Y.A. Bernard, E.J. Berquist, H.G.A. Burton, A. Carreras, K. Carter-Fenk, R. Chakraborty, A.D. Chien, K.D. Closser, V. Cofer-Shabica, S. Dasgupta, M. de Wergifosse, J. Deng, M. Diedenhofen, H. Do, S. Ehlert, P.-T. Fang, S. Fatehi, Q. Feng, T. Friedhoff, J. Gayvert, Q. Ge, G. Gidofalvi, M. Goldey, J. Gomes, C.E. González-Espinoza, S. Gulania, A.O. Gunina, M.W.D. Hanson-Heine, P.H.P. Harbach, A. Hauser, M.F. Herbst, M. Hernández Vera, M. Hodecker, Z.C. Holden, S. Houck, X. Huang, K. Hui, B.C. Huynh, M. Ivanov, A. Jász, H. Ji, H. Jiang, B. Kaduk, S. Kähler, K. Khistyaev, J. Kim, G. Kis, P. Klunzinger, Z. Koczor-Benda, J.H. Koh, D. Kosenkov, L. Koulias, T. Kowalczyk, C.M. Krauter, K. Kue, A. Kunitsa, T. Kus, I. Ladjánszki, A. Landau, K.V. Lawler, D. Lefrancois, etal, J. Chem. Phys. **155**, 084801 (2021). doi:10.1063/5.0055522
[56] A. Botti, S.E. Pagnotta, F. Bruni and M.A. Ricci, J. Phys. Chem. B **113**, 10014 (2009). doi:10.1021/jp903462h
[57] H.M. Senn and W. Thiel, Angew. Chem. Int. Ed. **48**, 1198 (2009). doi:10.1002/anie.200802019
[58] Y.-W. Hsiao, Y. Tao, J.E. Shokes, R.A. Scott and U. Ryde, Phys. Rev. B **74**, 214101 (2002). doi:10.1103/PhysRevB.74.214101
[59] A. Genoni, L. Bučinský, N. Claiser, J. Contreras-Garcíia, B. Dittrich, P.M. Dominiak, E. Espinosa, C. Gatti amd, P. Giannozzi, J.-M. Gillet, D. Jayatilaka, P. Macchi, A.O. Madsen, L. Massa, C.F. Matta, K.M. Merz Jr., P.N.H. Nakashima, H. Ott, U. Ryde, K. Schwarz, M. Sierka and S. Grabowsky, Chem. Eur. J **24**, 10881 (2018). doi:10.1002/chem.v24.43
[60] J. Bergmann, E. Oksanen and U. Ryde, Curr. Op. Struct. Biol. **72**, 18 (2022). doi:10.1016/j.sbi.2021.07.002
[61] F. Plasser, A.I. Krylov and A. Dreuw, WIREs: Comput. Mol. Sci. **12**, e1595 (2022). doi:10.1002/wcms.1546.
[62] S. Mewes, F. Plasser, A.I. Krylov and A. Dreuw, J. Chem. Theory Comput. **14**, 710 (2018). doi:10.1021/acs.jctc.7b01145
[63] D. Ghosh, O. Isayev, L.V. Slipchenko and A.I. Krylov, J. Phys. Chem. A **115**, 6028 (2011). doi:10.1021/jp110438c
[64] S. Gozem, R. Seidel, U. Hergenhahn, E. Lugovoy, B. Abel, B. Winter, A.I. Krylov and S.E. Bradfort, J. Phys. Chem. Lett. **11**, 5162 (2020). doi:10.1021/acs.jpclett.0c00968